DOI: 10.1093/jnci/djr523
Advance Access publication on January 13, 2012.

ARTICLE

Effect of *KRAS* Oncogene Substitutions on Protein Behavior: Implications for Signaling and Clinical Outcome

Nathan T. Ihle, Lauren A. Byers, Edward S. Kim, Pierre Saintigny, J. Jack Lee, George R. Blumenschein, Anne Tsao, Suyu Liu, Jill E. Larsen, Jing Wang, Lixia Diao, Kevin R. Coombes, Lu Chen, Shuxing Zhang, Mena F. Abdelmelek, Ximing Tang, Vassiliki Papadimitrakopoulou, John D. Minna, Scott M. Lippman, Waun K. Hong, Roy S. Herbst, Ignacio I. Wistuba, John V. Heymach, Garth Powis

Manuscript received March 29, 2011; revised October 28, 2011; accepted November 22, 2011.

Correspondence to: Garth Powis, DPhil, Department of Experimental Therapeutics, MD Anderson Cancer Center, 1400 Holcombe Blvd, FC6.3044, Unit 422, Houston, TX 77030 (e-mail: gpowis@mdanderson.org).

Background Mutations in the v-Ki-ras2 Kirsten rat sarcoma viral oncogene homolog (*KRAS*) play a critical role in cancer cell growth and resistance to therapy. Most mutations occur at codons 12 and 13. In colorectal cancer, the presence of any mutant KRas amino acid substitution is a negative predictor of patient response to targeted therapy. However, in non–small cell lung cancer (NSCLC), the evidence that *KRAS* mutation is a predictive factor is conflicting.

Methods We used data from a molecularly targeted clinical trial for 215 patients with tissues available out of 268 evaluable patients with refractory NSCLC to examine associations between specific mutant KRas proteins and progression-free survival and tumor gene expression. Transcriptome microarray studies of patient tumor samples and reverse-phase protein array studies of a panel of 67 NSCLC cell lines with known substitutions in KRas and in immortalized human bronchial epithelial cells stably expressing different mutant KRas proteins were used to investigate signaling pathway activation. Molecular modeling was used to study the conformations of wild-type and mutant KRas proteins. Kaplan–Meier curves and Cox regression were used to analyze survival data. All statistical tests were two-sided.

Results Patients whose tumors had either mutant KRas-Gly12Cys or mutant KRas-Gly12Val had worse progression-free survival compared with patients whose tumors had other mutant KRas proteins or wild-type KRas ($P = .046$, median survival = 1.84 months) compared with all other mutant KRas (median survival = 3.35 months) or wild-type KRas (median survival = 1.95 months). NSCLC cell lines with mutant KRas-Gly12Asp had activated phosphatidylinositol 3-kinase (PI-3-K) and mitogen-activated protein/extracellular signal-regulated kinase kinase (MEK) signaling, whereas those with mutant KRas-Gly12Cys or mutant KRas-Gly12Val had activated Ral signaling and decreased growth factor–dependent Akt activation. Molecular modeling studies showed that different conformations imposed by mutant KRas may lead to altered association with downstream signaling transducers.

Conclusions Not all mutant KRas proteins affect patient survival or downstream signaling in a similar way. The heterogeneous behavior of mutant KRas proteins implies that therapeutic interventions may need to take into account the specific mutant KRas expressed by the tumor.

J Natl Cancer Inst 2012;104:228–239

Approximately 30% of all human cancers have a mutation in the v-Ki-ras2 Kirsten rat sarcoma viral oncogene homolog (*KRAS*), which encodes a GTPase that is essential for normal signaling; mutant *KRAS* plays a critical role in cancer cell growth and resistance to therapy (1). In colorectal cancer, the presence of a *KRAS* mutation predicts resistance to therapies that target the epidermal growth factor receptor (EGFR) and is predictive of poor prognosis (2). Less clear is the role of *KRAS* mutations as a predictive factor in non–small cell lung cancer (NSCLC): Some studies have shown a weak association with resistance to treatment and other studies have shown no association (3).

KRAS mutations in patient tumors are limited to a few sites; most mutations occur in codon 12, whereas codons 13, 10, and 61 are much less frequently mutated (1). Codon 12 or 13 *KRAS* mutations result in base changes that lead to amino acid substitutions that lock the KRas protein in an active state (4). The frequency and spectrum of *KRAS* mutations in codons 12 and 13 differs among cancer types. For example, the most common *KRAS*

mutation in colorectal tumors, as in most solid tumors including NSCLCs in nonsmoking patients, is a G to A transition (92% of mutations); a G to A transition at codon 12 and/or codon 13 results in KRas proteins in which the wild-type glycine (Gly) residue is replaced by an aspartate (Asp; approximately 50% of tumors), a valine (Val; 28% of tumors), or a cysteine (Cys; 9% of tumors) (1,5,6). In NSCLC in patients who smoke, the most common *KRAS* mutation is a G to T transversion (84% of mutations), and the most common amino acid replacements at codon 12 and/or codon 13 are Cys (47% of tumors), Val (24%), Asp (15%), and alanine (7%) (1,6–8).

KRas has the ability to activate multiple downstream signaling pathways that have been implicated as independent drivers of tumorigenesis, including those involving phosphatidylinositol 3-kinase (PI-3-K), mitogen-activated protein/extracellular signal-regulated kinase kinase (MEK), v-ral simian leukemia viral oncogene homolog ras related (Ral), mammalian target of rapamycin (mTOR), and p70 S6 kinase (9). In this study, we used data from a recently completed biopsy-required, biomarker-driven, molecularly targeted multi-arm trial in patients with refractory NSCLC to examine the associations between mutant KRas proteins bearing different amino acid substitutions and patient response to molecularly targeted therapy. We analyzed tumor transcriptome microarray data for expression of cell cycle genes. We used a panel of NSCLC cell lines with known amino acid substitutions in KRas to identify pathways activated by the different mutant KRas proteins. Finally, we used molecular modeling to examine interactions between wild-type and mutant KRas proteins and downstream signaling transducers.

CONTEXT AND CAVEATS

Prior knowledge

KRas protein is a GTPase involved in signal transduction, and mutant KRas plays a critical role in cancer cell growth and resistance to therapy. Mutant KRas proteins with any amino acid substitution are a negative predictor of patient response to targeted therapy in colorectal cancer. However, there is inconsistent evidence that mutant *KRAS* is a predictive factor in non–small cell lung cancer (NSCLC).

Study design

Data from a clinical trial of patients with refractory NSCLC were used to examine associations between specific mutant KRas proteins and patient response to molecularly targeted therapy and tumor gene expression. Microarray analysis was used to identify signaling pathways activated in 67 NSCLC lines that expressed different mutant KRas proteins.

Contribution

Mutant KRas-Gly12Cys and mutant KRas-Gly12Val were associated with decreased progression-free survival compared with other mutant KRas or wild-type KRas. NSCLC cell lines with mutant KRas-Gly12Asp had activated phosphatidylinositol 3-kinase and mitogen-activated protein/extracellular signal-regulated kinase kinase signaling, whereas those with mutant KRas-Gly12Cys or mutant KRas-Gly12Val had activated Ral signaling and decreased growth factor–dependent Akt activation.

Implication

Therapeutic interventions may need to take into account the specific mutant KRas protein expressed by the tumor.

Limitations

Only the major forms of mutant KRas in NSCLC and three downstream signaling pathways were considered. The patient response results may only be applicable to the types of molecularly targeted agents used in the clinical trial.

From the Editors

Methods

BATTLE Clinical Trial

To analyze associations between specific mutant KRas amino acid substitutions and patient survival, we used data from the prospective phase II Biomarker-integrated Approaches of Targeted Therapy for Lung Cancer Elimination (BATTLE) trial in patients with refractory NSCLC who had agreed to a baseline tumor biopsy (10). The BATTLE trial used an adaptive method to randomly assign patients with refractory NSCLC who agreed to a have a baseline biopsy of their tumor to one of four trial arms testing treatments with erlotinib, vandetanib, bexarotene and erlotinib, or sorafenib. The primary endpoint of the trial was disease control rate at 8 weeks. Radiographic imaging of tumors was reviewed to determine suitability of patients for biopsy. Patients who were 18 years of age or older and had an adequate performance status (Eastern Cooperative Oncology Group grade 0–2) were eligible for the trial. Although previous treatment with erlotinib was allowed, patients who had received erlotinib were excluded from the erlotinib-containing study arms. Patients with stable (for at least 4 weeks) or treated brain metastases were included in the trial. All participants provided written informed consent. The BATTLE trial enrolled 341 patients, and, among them, 255 were randomly assigned. Of the 341 patients enrolled, 268 had tumor tissue available for *KRAS* mutation analysis, and of these, 48 had a mutant *KRAS* in their tumor. Of the 255 patients who were randomly assigned, 215 had tumor tissue available for *KRAS* mutation analysis and were also evaluable for the progression-free survival.

Microarray Analysis of Patient Tumor Gene Expression Profiles

We conducted microarray analysis of mRNA expression on frozen tumor core biopsy samples from 101 patients who had been randomly assigned to a BATTLE treatment arm (27 to erlotinib, eight to erlotinib and bexarotene, 47 to sorafenib, and 19 to vandetanib) and were evaluable for 8-week disease control. Core tumor biopsy samples were taken from each patient before treatment at either the primary lung tumor or a metastatic site. Approximately one-third of the core from each sample was used for total RNA extraction and global gene expression analysis. RNA was extracted from tissue embedded in Tissue-Tek OCT compound (Ted-Pella Inc, Reding, CA) using the RNeasy Mini Kit (Qiagen, Valencia, CA) including on-column DNase (Qiagen, Valencia, CA) digestion as described by the manufacturer's protocol. Hematoxylin- and eosin-stained sections of all of the samples were available to check for the presence of cancer cells. RNA

quantification was done using a Nanodrop Technologies ND-1000 spectrophotometer (Thermo Scientific, Wilmington, DE). All RNA samples were serially diluted in RNAse-free water to obtain a 250-pg/μL stock solution. RNA quality was ensured by analyzing a separation trace of RNA using the RNA6000 PicoAssay for the Bioanalyzer 2100 (Agilent Technologies, Palo Alto, CA). Aliquots of RNA were prepared and stored at −80°C. Each aliquot was used once. The decision to submit the RNA sample for amplification was based on its purity (ie, ratio of the absorbance at 260 nm to that at 280 nm [260/280 ratio] ≥2.0), and an RNA integrity number (RIN) greater than 7 or when the RIN number was low or not available, the presence of an electrophoretic trace on a case-by-case basis. We used 0.5–50 ng of RNA for amplification, which was performed using a WT-Amplification Pico kit (NuGEN, San Carlos, CA). The amplification products were labeled using an FL-Ovation cDNA Biotin Module V2 (NuGEN) according to the manufacturers' protocols. The quantity and quality of the amplified cRNA was reassessed with the use of an ND 1000 spectrophotometer and Agilent Bioanalyzer (Agilent Technologies). When the RIN was lower than 7, amplification and labeling were repeated. Hybridization mixtures were prepared according to Affymetrix procedures (Affymetrix, Santa Clara, CA) to accommodate 5 μg of cDNA targets from NuGEN amplification with an RNA integrity number greater than 7. Hybridization was performed with the use of a Human Gene 1.ST platform (Affymetrix) according to the manufacturer's protocols. All steps from hybridization to the generation of raw microarray data were carried out at the University of Texas MD Anderson Cancer Center Microarray and Affymetrix Facility. Gene chips were scanned using an Affymetrix 7G scanner (Affymetrix), and images (DAT files) were converted to CEL files using GCOS software (Affymetrix).

Cells and Culture Conditions

A panel of 67 NSCLC cell lines (11,12) were provided by Dr J. D. Minna and grown in RPMI-1640 medium (Hyclone, Logan, UT) with 10% fetal bovine serum (FBS; Aleken Biologicals, Nash, TX) as previously described. Immortalized human bronchial epithelial cells with specific short hairpin RNA (shRNA) knockdown of p53 mRNA (HBECsiP53) (13,14) were maintained in K-SFM medium containing 50 μg/mL of bovine pituitary extract (BPE) and 5 ng/mL of epidermal growth factor (EGF) (all from Life Technologies, Carlsbad, CA). All cell lines were tested to confirm the absence of mycoplasma using an e-Myco PCR detection kit (Boca Scientific, Boca Raton, FL). The identities of the NSCLC cell lines were confirmed through DNA fingerprinting by the University of Texas MD Anderson Cancer Center Characterized Cell Line Core Service at the time of total protein lysate preparation. Mutant *KRAS*-transfected HBECsiP53 were sequenced to confirm the specific *KRAS* mutation (Supplementary Figure 1, available online).

Preparation of Protein Lysates and Reverse-Phase Protein Array (RPPA)

For each cell line including HBECsiP53, we prepared a protein lysate from cells harvested from subconfluent cultures that were incubated for 24 hours in medium containing no or 10% FBS. For total protein lysate preparation, the medium was removed, and the cells were washed twice with ice-cold phosphate-buffered saline (PBS)–containing Complete protease inhibitor cocktail tablets and PhosSTOP Phosphatase inhibitor cocktail tablets (two tablets each per 500 mL PBS; Roche Applied Science, Mannheim, Germany) and 1 mM Na_3VO_4. Lysis buffer (1% Triton X-100, 50 mM HEPES [pH 7.4], 150 mM NaCl, 1.5 mM $MgCl_2$, 1 mM EGTA, 100 mM NaF, 10 mM $Na_4P_2O_7$, 10% glycerol, 1 mM phenylmethylsulfonyl fluoride, 1 mM Na_3VO_4, and 10 μg/mL aprotinin) was added to the cells, and samples were vortexed frequently on ice for 20 minutes, followed by microcentrifugation at 18 000*g* for 10 minutes. Cleared supernatants were collected, and protein was measured using a BCA protein assay kit (Pierce Biotechnology Inc, Rockford, IL). Specific signaling proteins and phosphoproteins were then quantified by RPPA, using mouse monoclonal antibodies specifically validated for RPPA use (listed in Supplementary Table 1, available online) at optimized concentrations as previously described (12). Lysate was applied to slides for RPPA analysis. For each cell line, a serial dilution of five concentrations of the lysate was deposited on slides using a pin-based Aushon's 2470 microarrayer (Aushon Biosystems, Billerica, MA), with 10% of the samples replicated for quality control. Immunostaining was performed with the use of an automated autostainer (BioGenex, San Ramon, CA). Each array was incubated with primary antibody, and signal was detected using a catalyzed signal amplification system (Dako Cytomation California Inc, Carpinteria, CA). After quantification, the data were logarithmically transformed (base 2) for further processing and analysis.

Immunoblotting and Immunoprecipitation

Cells were washed twice with ice-cold PBS and then once with a lysis buffer containing 50 mmol/L HEPES (pH 7.5), 50 mmol/L NaCl, 0.2 mmol/L NaF, 0.2 mmol/L Na_3VO_4, 1 mmol/L phenylmethylsulfonyl fluoride, 20 μg/mL aprotinin, 20 μg/mL leupeptin, 1% Nonidet P-40, and 0.25% sodium deoxycholate. The protein concentration of each cell lysate was determined by the BCA protein assay (Pierce Biotechnology), and 50 μg of each lysate was boiled for 5 minutes in a denaturing buffer containing 0.25 mol/L Tris–HCl (pH 6.8), 35% glycerol, 8% sodium dodecyl sulfate, and 10% 2-mercaptoethanol, loaded on a 10% acrylamide–bisacrylamide gel, and resolved by electrophoresis at 150 V for 40 minutes. Proteins were electrophoretically transferred to a nitrocellulose membrane. The membrane was preincubated for 30 minutes in a blocking buffer (137 mmol/L NaCl, 2.7 mmol/L KCl, 897 mmol/L $CaCl_2$, 491 mmol/L $MgCl_2$, 3.4 mmol/L Na_2HPO_4, 593 mmol/L KH_2PO_4, and 5% bovine serum albumin) and then incubated overnight with rabbit monoclonal anti-phospho-Akt (Thr308), phospho-Akt (Ser473), anti-phospho-p70 S6 kinase (Thr389), or anti-Akt antibodies or rabbit polyclonal anti-phospho-Mapk (Thr202/Tyr204) antibodies (1:1000 dilution; Cell Signaling Technology, Danvers, MA). A goat polyclonal anti-lamin A/C antibody and a mouse monoclonal anti–β-actin antibody (Santa Cruz Biotechnology, Santa Cruz, CA) were used at 1:2000 dilution. Horseradish peroxidase–coupled donkey anti-rabbit immunoglobulin G secondary antibody (1:2000 dilution; GE Healthcare, Piscataway, NJ) was used for primary antibody detection, and a Western Lightening chemiluminescence kit (Perkin Elmer, Waltham, MA) was used to detect antibody

binding to the membrane. For measurement of active RalA and RalB, we used RalA and RalB activation kits (Millipore, Billerica, MA). Briefly, to measure active (ie, GTP-bound) RalA or RalB, HBECsiP53 cells were incubated for 1 hour at 4°C with Ral binding protein conjugated to beads. The beads were isolated by centrifugation at 18 000*g*, washed with PBS, denatured, and subjected to electrophoresis on polyacrylamide gels. RalA and RalB were detected by immunoblotting using a Renaissance chemiluminescence system (NEN, Boston, MA) on Kodak X-Omat Blue ML film (Eastman Kodak, Rochester, NY)

Lentiviral Vector Construction

Lentiviral vectors expressing wild-type *KRAS*, mutant *KRAS*-Gly12Cys, or mutant *KRAS*-Gly12Asp were constructed from a previously described vector, pLenti6-*KRAS*-V12 (14), using a site-directed mutagenesis kit (Stratagene, La Jolla, CA) according to the manufacturer's instructions. Correct sequences were confirmed by sequencing for all vectors. Viral transduction was performed as described previously (13) by transiently transfection of each viral vector into 293FT packaging cells with Viral Power Packaging Mix (Invitrogen, Carlsbad, CA) according to the manufacturer's instructions. Virus-containing medium was harvested 48–96 hours later and filtered through a 0.45-μm filter. HEBECsiP53 cells were stably infected with virus-containing media and 4 μg/mL polybrene (Sigma, St Loius, MO) for 16 hours followed by selection for 5 days in 2 μg/mL blasticidin (Invitrogen). All variants of *KRAS* were confirmed by DNA sequencing (Supplementary Figure 1, available online). RNA was extracted from the transformed cells and reverse transcribed to cDNA using an iScript cDNA Synthesis kit (Bio-Rad, Hercules, CA). cDNA was amplified using primers that bind either side of the codon 12 mutation (Forward primer: 5′-GACTGAATATAAACTTGTG GTAGTTGGACCT-3′; Reverse primer: 5′-TCCTCTTGACC TGCTGTGTCG-3′) and HotStar Taq polymerase (Qiagen, Germantown, MD), and the amplified products were purified with the use of a QiaQuick CleanUp kit (Qiagen, Germantown, MD). Products were sequenced using the forward primer and Big Dye Terminator v3.1 chemistry (Applied Biosystems, Foster City, CA) on an Applied Biosystems 3730xl instrument and purified with the use of Sephadex G-50 in Millipore Multiscreen plates (Millipore).

HBECsiP53 Plastic and Soft Agar Growth Assays

For cell growth assays on plastic, 2000 HBECsiP53 *KRAS*-transfected or wild-type cells were plated per well in 96-well plates (Griener, Monroe, SC) and allowed to attach for 16 hours. At various times up to 100 hours of growth, cell number was measured using phenazine methosulfate (Sigma-Aldrich, St Louis, MO) activation of methylthiazol tetrazolium (Promega, Madison, WI) and colorimetric measurement at 490 nm using a FLUOstar Omega Spectrometer (BMG Labtech, Cary, NC). Readings for eight wells were averaged per time point. Each plate contained four wells with no cells as a control background reading, which was subtracted from the samples from that plate. The experiment was performed in triplicate three times. Soft agar growth assays were performed as previously described (13). Briefly, HBECsiP53 cells were seeded at 1000 cells per well in 12-well plates in triplicate in K-SFM medium supplemented with 20% FBS, 50 μg/mL BPE, and 5 ng/mL EGF and incubated for 4 weeks. The cells were stained with 0.005% crystal violet and colonies (defined as >50 cells) were counted at ×4 magnification. Results are the average of three experiments.

Molecular Modeling

We retrieved the structures of Harvey rat sarcoma viral oncogene homolog (HRas) proteins in the PI-3-K/HRas complex (Protein Data Bank entry code: 1HE8) (15) and ral guanine nucleotide dissociation stimulator (RaLGDS)/HRas heterotetramer complex (Protein Data Bank entry code: 1LFD) (16) from the Protein Data Bank and used them as templates to build molecular models of wild-type KRas, mutant KRas-Gly12Cys, and mutant KRas-Gly12Asp. The homology models were energetically minimized using the NAMD software (17), and the resulting KRas homology models were superimposed to the HRas protein in 1HE8 and 1LFD, thus generating three PI-3-K/KRas complexes and three RaLGDS/KRas complexes. Molecular dynamics simulations of various forms of KRas in complex with PI-3-K or RaLGDS were carried out as previously described (14). The topology and parameter for GTP were generated as the chimeric analog of ATP and guanine using the CHARMM27 force field (18). Each protein complex was solvated in a water box in which every protein atom was at least 8 Å away from the boundary of the box. Sodium chloride at 100 mM was added to the water box to neutralize the system charges. Following equilibration of the system for 400 picoseconds, we then conducted 8-nanosecond molecular dynamics simulations while recording the trajectory (snapshot structures of the simulated system) every 200 femtoseconds. Trajectories of the last 6 nanoseconds for the six protein complexes were superimposed using the WORDOM software (19). The average structure for each protein complex was calculated with WORDOM and then optimized with the carbon-tethered energy minimization method of the Molecular Operating Environment software package (Chemical Computing Group, Montreal, Canada) to reduce structural defects. The snapshot structures of each protein complex were taken every 100 picoseconds, and we used the ZRANK program (20) to calculate the ZRANK score, an estimate of the relative binding affinities of different forms of KRas to PI-3-K or RaLGDS in which a lower score indicates tighter binding.

Statistical Analysis

Descriptive statistics were used to summarize all data. Dot plots, bar charts, and box plots were used where appropriate to provide a graphic assessment of the distributions of the data. Colony numbers for the soft agar growth assay for different cell line groups were compared using one-way analysis of variance. The Kaplan–Meier method was used to estimate the survival function for progression-free survival, and multivariable Cox regression analysis was applied to the patient survival data. The effects of multiple treatments, subtypes of KRas mutation, and their interactions were controlled for by Cox regression. Unsupervised cluster analysis was used for the microarray and RRPA data using the Pearson correlation distance between proteins, Euclidean distance between cell lines, and Ward linkage rule. The statistical analyses of microarray data were performed using R Development

Core Team (version 2.7.0, 2010; R Foundation for Statistical Computing, Vienna, Austria. ISBN 3-900051-07-0; URL http://www.R-project.org). RRPA data were logarithmically transformed (base 2) for processing and analysis. We chose a somewhat arbitrary false discovery rate of 0.3 because it struck a good balance between the number of statistically significant markers and a reasonable *P* value threshold for statistical significance. As a result, we selected 66 statistically significant markers, with a corresponding *P* value of .015, for the cluster analysis. All statistical tests were performed with a two-sided 5% type I error rate.

Results

Association Between KRas Proteins and NSCLC Patient Survival

The recently completed BATTLE trial for patients with refractory NSCLC who received either erlotinib, vandetanib, bexarotene and erlotinib, or sorafenib reported that grouping all *KRAS* mutations together was not associated with either overall survival or progression-free survival (*P* = .086) (10). We examined whether specific *KRAS* mutations were associated with survival. Of the 341 patients enrolled in the BATTLE trial, 268 had tumor *KRAS* mutation analysis performed. Of those patients, 48 had a *KRAS* mutation: one patient (2%) had a mutation at codon 10, 42 (88%) had a mutation at codon 12, two (4%) had a mutation at codon 13, and three (6%) had a mutation at codon 61 (Table 1). We also analyzed the BATTLE data for the association between different amino acid substitutions in mutant KRas and progression-free survival. Among the 255 patients who were randomly assigned to a treatment group, 215 had tissues available for the *KRAS* mutation analysis and were evaluable for the progression-free survival. We found that 43 patients had mutant KRas: 24 patients had Cys or Val substitution at codon 12 and 19 patients had other amino acids substitutions at codon 12 (Figure 1, A). Mutant KRas-Gly12Cys and KRas-Gly12Val was associated with a statistically significantly decreased progression-free survival (*P* = .046, median survival = 1.84 months) compared with all other mutant KRas (median survival = 3.35 months) or wild-type KRas (median survival = 1.95 months) (Figure 1, A). The negative association between a Cys or Val substitution at codon 12 and progression-free survival was most pronounced for patients in the sorafenib treatment arm (*P* = .026) (Figure 1, B). Although only three patients in the vandetanib arm had either mutant KRas-Gly12Cys or mutant KRas-Gly12Val, we observed a statistically significant association between these mutations and with decreased progression-free survival (*P* = .001). There was no association between tumors that expressed mutant KRas-Gly12Cys or mutant KRas-Gly12Val and progression-free survival in either erlotinib treatment arm; we suspect this is because of the high incidence of multiple EGFR mutations that was seen in the NSCLC patients in the BATTLE trial (10).

Table 1. KRas mutation status of all BATTLE* trial patients with available tumor tissue (n = 268)

Amino acid substitution or mutated codon	Patient population distribution		
	Cys or Val (n = 26)	Other amino acid (n = 22)	Wild type (n = 220)
Amino acid at codon of interest			
Gly	0	0	220
Ala	0	5	0
Asp	0	11	0
Cys	17	0	0
Val	8	0	0
Cys and Val	1	0	0
Other	0	6	0
Mutated codon			
None	0	0	220
10	0	1	0
12	26	16	0
13	0	2	0
61	0	3	0

* BATTLE stands for Biomarker-based Approaches of Targeted Therapy for Lung Cancer Elimination. This is a biomarker-based adaptive random trial in stage IV recurrent non–small cell lung cancer patients to evaluate the 8-week disease control rate of four regiments of targeted agents.

Tumor Microarray Transcriptome Analysis

We next performed a supervised cluster analysis of microarray transcriptome data from tumors from the BATTLE trial to identify genes whose expression differed statistically significantly between tumors that expressed either mutant KRas-Gly12Cys or mutant KRas-Gly12Val and those that expressed other mutant forms of KRas. We identified genes that most accurately defined the differences between these two mutant KRas groups, thereby allowing clustering of the patients into two groups (Figure 1, C; Supplementary Data, available online). Genes that defined the two groups included the cell cycle regulators *PLK1* (polo-like kinase 1), *CCNB1* (cyclin B), and *CCNE1* (cyclin E), whose expression was lower in tumors expressing either mutant KRas-Gly12Cys or mutant KRas-Gly12Val and higher in the remaining mutant KRas tumors, compared with tumors expressing wild-type KRas.

Effect of Mutant Forms of KRas on Downstream Signaling in NSCLC Cell Lines

To examine the effect of mutant forms of KRas on protein signal transduction, we conducted a comprehensive RRPA analysis across a panel of 67 genetically characterized NSCLC cell lines comparing specific signaling protein expression in lines that expressed either mutant KRas-Gly12 or 13 Cys or mutant KRas-Gly12Val (n = 13 cell lines), with cell lines that expressed any other mutant KRas (n = 9 cell lines) and wild-type KRas (n = 45 cell lines). Neither phosphorylated Mek nor phosphorylated p38 showed statistically significant differences in expression levels between cell lines that had either mutant KRas-Gly12Cys or mutant KRas-Gly12Val, and those that had other mutant forms of KRas or wild-type KRas (Figure 2, A and B). However, phosphorylated Akt levels were decreased in cell lines that expressed either mutant KRas-Gly12Cys or mutant KRas-Gly12Val compared with cells lines that expressed other mutant KRas (*P* = .009) or wild-type KRas (*P* = .020) (Figure 2, C). These findings were confirmed by immunoblot analysis of whole-cell lysates for a set of seven NSCLC cell lines with KRas codon 12 mutations (Figure 2, D).

To study the signaling and growth effects of different KRas mutations in a uniform cell background, we stably expressed the

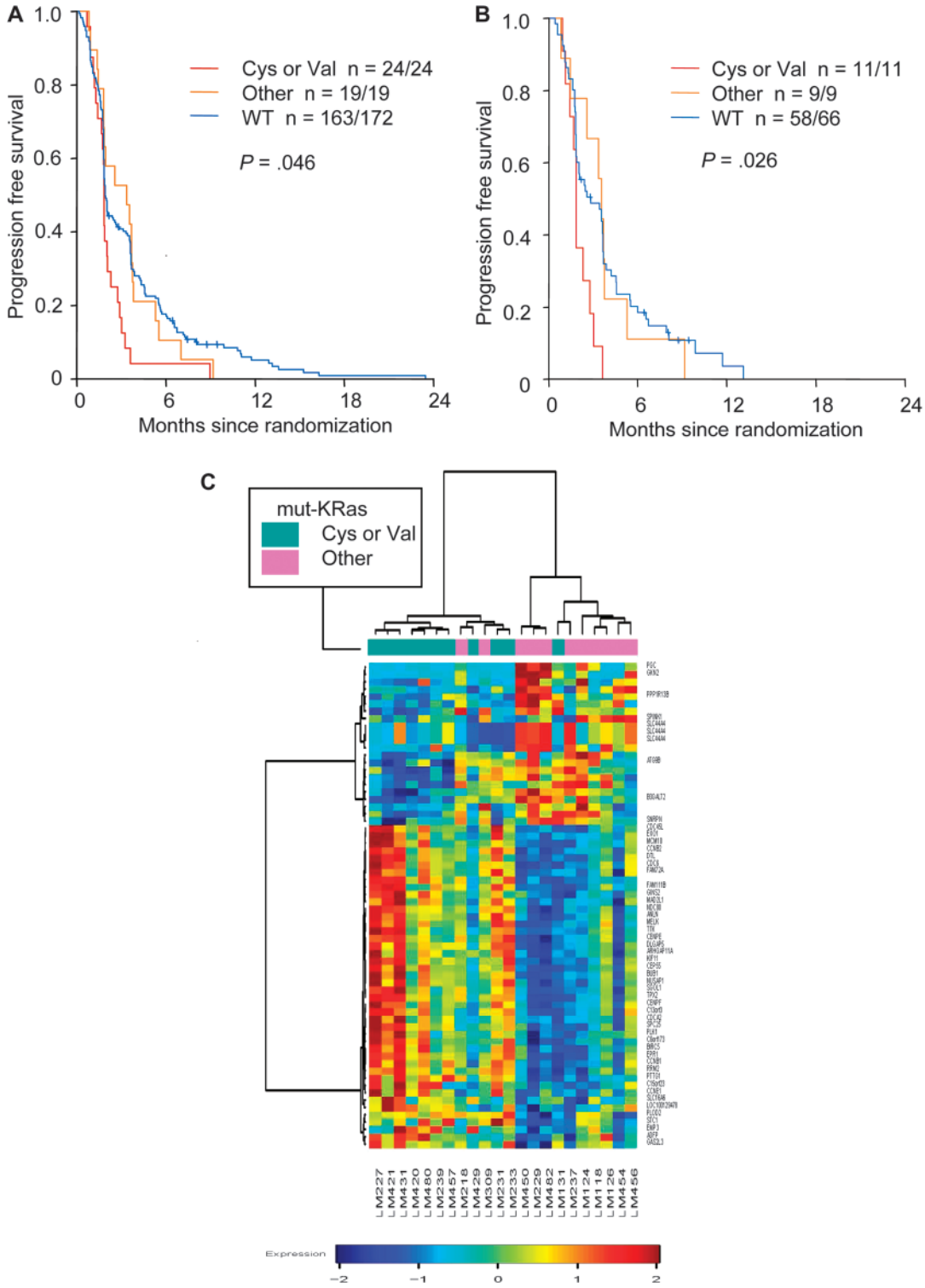

Figure 1. Mutant KRas-Gly12Cys and mutant KRas-Gly12Val and response in refractory non–small cell lung cancer (NSCLC). Kaplan–Meier plots of progression-free survival (PFS) for NSCLC patients in the BATTLE trial by tumor KRas mutation for (**A**) all treatments and (**B**) for sorafenib-treated patients. n = *a*/*b* indicates "*a*" total number of events in "*b*" patients in each category. Data were analyzed by the log-rank test. *P* values are two-sided. **C**) Cluster analysis of microarray data from patients treated in BATTLE trial of genes that most accurately define the differences between mutant KRas-Gly12Cys or mutant KRas-Gly12Val, and other mutant KRas tumors. The false discovery rate was chosen as 0.3. **Red dots** indicate genes known to be involved in cell cycle regulation. Panel A: The numbers at risk at 3, 6, and 12 months were 4, 1, 0 for Cys/Val; 10, 2, 0 for other; and 67, 29, 6 for wild-type KRas groups, respectively. The corresponding PFS (95% confidence intervals [CIs]) were 0.17 (95% CI = 0.07 to 0.41), 0.04 (95% CI = 0.01 to 0.28), and NA (not applicable) for the Cys/Val group; 0.53 (95% CI = 0.34 to 0.81), 0.11 (95% CI = 0.03 to 0.39), and NA for the other group; and 0.41 (95% CI = 0.34 to 0.49), 0.18 (95% CI = 0.13 to 0.25), and 0.05 (95% CI = 0.02 to 0.11) for the wild-type KRas group. Panel B: The numbers at risk at 3, 6, and 12 months were 2, 0, 0 for Cys/Val; 6, 1, 0, for other; and 29, 12, 1, for wild-type KRas groups, respectively. The corresponding PFS (95% CIs) were 0.18 (95% CI = 0.05 to 0.64), NA (NA) for the Cys/Val group; 0.67 (95% CI = 0.42 to 1.00), 0.11 (95% CI = 0.02 to 0.71), and NA for the other group; and 0.49 (95% CI = 0.38 to 0.63), 0.20 (95% CI = 0.12 to 0.33), and 0.04 (95% CI = 0.01 to 0.21) for the wild-type KRas group.

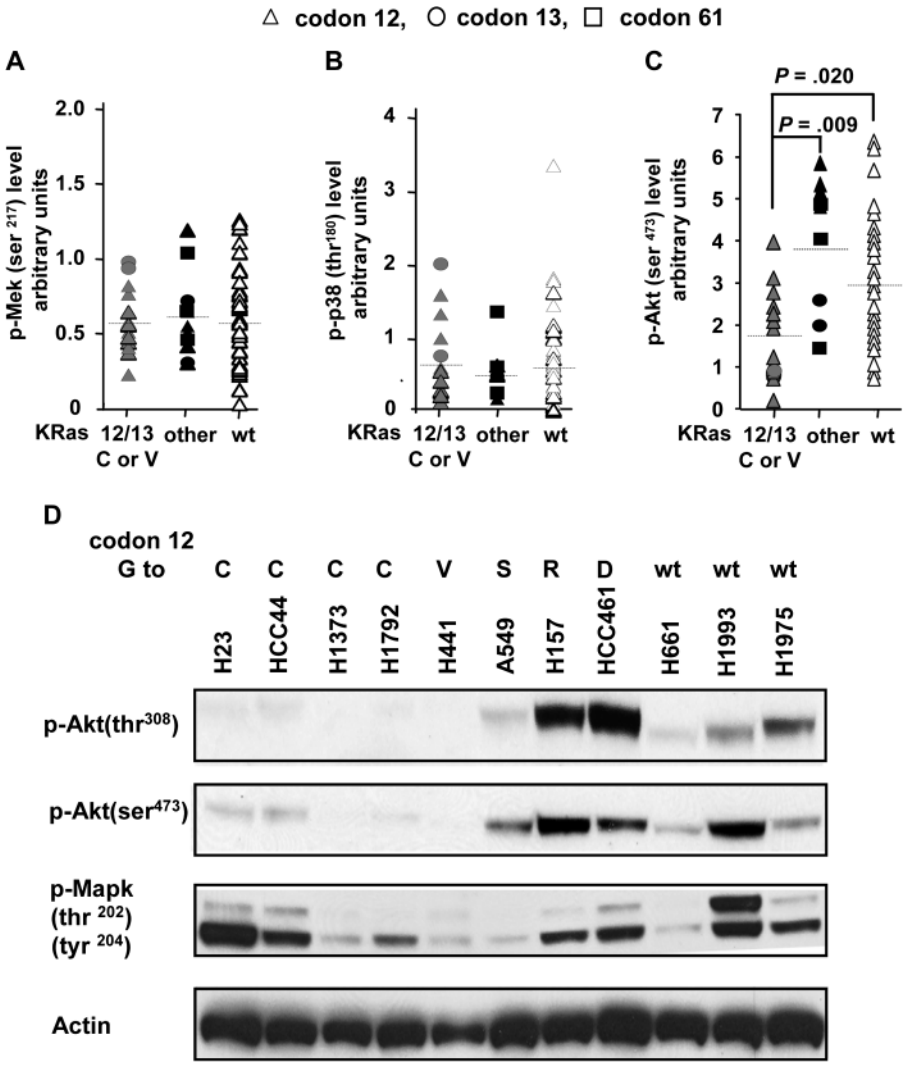

Figure 2. Mek and Akt signaling in non–small cell lung cancer (NSCLC) cell lines expressing mutant or wild-type KRas. Reverse-phase protein array levels of (**A**) phospho-Mek (ser^{217}), (**B**) phospho-p38 (thr^{180}), and (**C**) phospho-Akt (ser^{473}) for a panel of 67 NSCLC cell lines expressing mutant or wild-type KRas. KRas 12/13 C or V = cell lines with mutant KRas-Gly12Cys or mutant KRas-Gly13Cys (n = 13) or mutant KRas-Gly12Val (n = 1); other = cell lines with other mutant KRas (n = 9), wt = cell lines with wild-type KRas (n = 45). **Horizontal bars** indicate the mean value for the group. *P* values are two-sided (Wilcoxon rank test). **D**) Immunoblot analysis of a smaller panel of 11 NSCLC cell lines expressing mutant KRas with different codon 12 amino acid substitutions or wild-type KRas with Gly (G) at codon 12. C = Cys; D = Asp; R = Arg; S = Ser; V = Val.

most common mutant KRas in colon cancer (KRas-Gly12Asp), the most common mutant KRas in NSCLC (KRas-Gly12Cys), and wild-type KRas in previously characterized immortalized human bronchial epithelial cells (13) with shRNA knockdown of p53 to repress the toxicity of KRas in transformed cells (HBECsiP53). The DNA from the expression plasmids was sequenced for all the cell lines to ensure that the plasmids were expressed and that mutant KRas was present (Supplementary Figure 1, available online). HBECsiP53 cells that expressed wild-type KRas or either mutant KRas grew at similar rates in two-dimensional culture on plastic surfaces, and all three grew faster than cells transfected with empty vector (Figure 3, A). However, HBECsiP53 cells expressing mutant KRas-Gly12Cys showed statistically significantly increased anchorage-independent growth measured by colony formation in soft agarose compared with HBECsiP53 cells expressing mutant KRas-Gly12Asp ($P = .008$) or cells expressing wild-type KRas ($P < .001$) (Figure 3, B). Immunoblot analysis revealed that HBECsiP53 cells expressing mutant KRas-Gly12Asp had elevated levels of phosphorylated Akt compared with cells expressing wild-type KRas or empty vector, whereas cells that expressed wild-type KRas or mutant KRas-Gly12Cys had decreased levels of phosphorylated Akt compared with mutant KRas-Gly12Asp cells (Figure 4, C). The KRas downstream effectors RalA and RalB were both found to be activated in HBECsiP53 cells that expressed mutant KRas-Gly12Cys or wild type KRas, but not in cells that expressed mutant KRas-Gly12Asp (Figure 3, D). The results suggest that different amino acid substitutions in mutant KRas may activate different downstream signaling pathways compared with wild-type KRas (ie, mutant KRas-Gly12Asp through phospho-Akt signaling and mutant KRas-Gly12Cys through Ral signaling).

mTOR and Akt Signaling in NSCLC Cell Lines Expressing Mutant KRas Proteins

Mutant KRas and growth factors both lead to Akt phosphorylation, which results in mTOR activation and increased protein translation and tumorigenesis (21). mTOR activation also leads to feedback repression of growth factor–mediated Akt signaling through its effector p70 S6 kinase. Because Gly12Cys is the predominant KRas mutation in lung cancer (5,7,8), we were intrigued by the lack of Akt phosphorylation in HBECsiP53 cells expressing mutant KRas-Gly12Cys, even though these cells were grown in the presence of FBS. We therefore examined growth factor

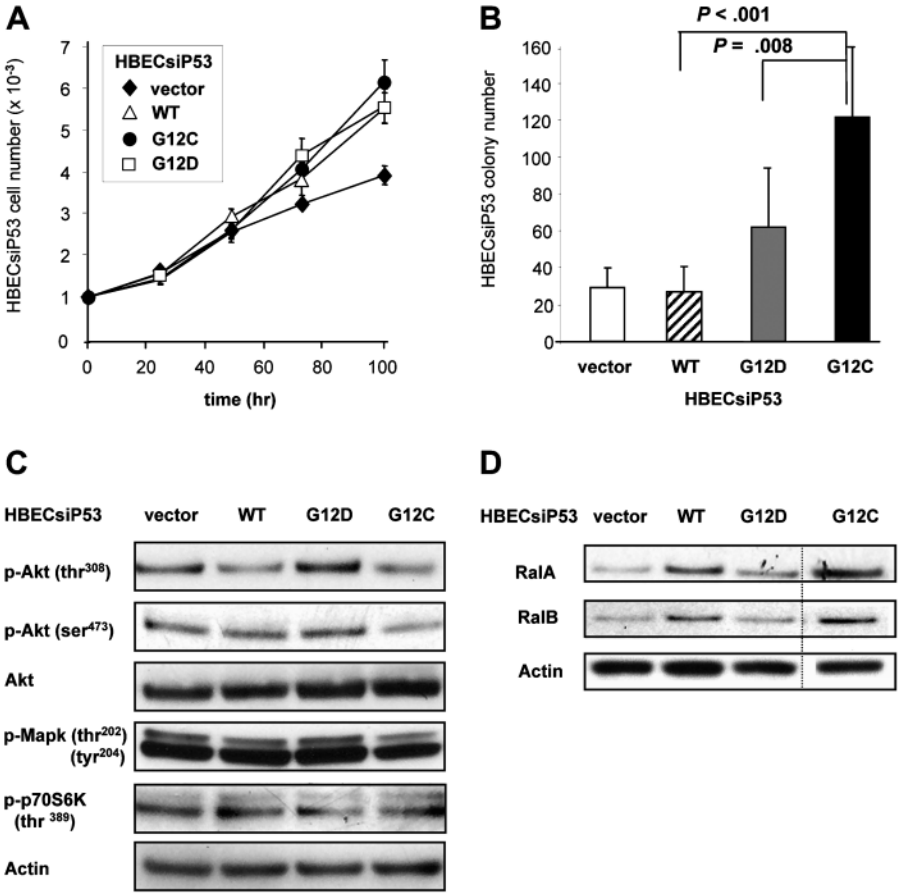

Figure 3. Signaling pathway activation in immortalized human bronchial epithelial cells with short hairpin RNA knockdown of p53 (HBECsiP53) stably transfected with *KRAS* expression plasmids. HBECsiP53 cells stably transfected with empty vector (vector), or vector coding for wild-type KRas (WT), mutant KRas-Gly12Cys (G12C), or mutant KRas-Gly12Asp (G12D) were grown on a plastic surface for 100 hrs (**A**) or in soft agarose for 4 weeks to assess anchorage-independent growth (**B**). Values are the mean of three experiments; **error bars** represent 95% confidence intervals. *P* values are two-sided (analysis of variance). **C**) Immunoblot analysis of Akt and Mapk pathway activation in the transfected HBECsiP53 cell lines. **D**) Pull-down assay for active RalA and RalB in the transfected HBECsiP53 cell lines. The experiments were repeated at least three times with similar results.

(ie, FBS)–mediated activation (ie, phosphorylation) of Akt as well as levels of phosphorylated p70 S6 kinase, which represses Akt activation by growth factors, in HBECsiP53 cells that expressed different mutant KRas proteins.

Despite the lower levels of phosphorylated Akt seen in NSCLC or HBEcsiP53 cells expressing either mutant KRas-Gly12Cys or mutant KRas-Gly12Val (Figures 1, C and 3, C), the levels of the mTOR effectors phospho-p70S6K and 4EBP were not statistically significantly changed compared with other mutant KRas or wild-type KRas cells (Figure 4, A and B). To examine the relationship between activation of the Akt pathway and mTOR activation, we subjected a panel of mutant KRas NSCLC cell lines to hierarchical clustering based on activation of downstream targets of Akt and mTOR signaling (Figure 4, B). We observed that NSCLC cells expressing mutant KRas-G12 or G13Cys or mutant KRas-G12Val had low levels of phospho-Akt (Figure 2, C) and no activation of phospho-Mek or phospho-p38, without or with serum (Supplementary Figure 2, available online). However, in the presence of serum, cell lines with mutant KRas-Gly12Cys or KRas-Gly12Val exhibited robust activation of the mTOR effector protein p70 S6 kinase compared with cell lines that expressed other mutant KRas proteins ($P = .02$) or wild-type KRas ($P = .01$). To determine if this p70 S6 kinase activation with KRas-Gly12Cys or KRas-Gly12Val contributed to our observation that mutant KRas-Gly12Cys or G12Val resulted in lower Akt activation, we treated KRas-transfected HBECsiP53 cell lines with the mTOR inhibitor rapamycin and examined its effects on signaling (Figure 4, C). Rapamycin inhibited activation of p70 S6 kinase in all of the transfected HBECsiP53 cell lines but induced activation of Akt in HBECsiP53 cells expressing wild-type KRas or mutant KRas-Gly12Cys. However, in HBECsiP53 cells expressing mutant KRas-Gly12Asp, Akt was constitutively activated, and rapamycin did not further increased the level of phosphorylated Akt, indicating that in these cells there was constitutive growth factor–independent activation of the signaling. Rapamycin had comparable effects on Akt activation in NSCLC cell lines expressing wild-type KRas, mutant KRas-Gly12Cys, and mutant KRas-Gly12Asp (Figure 4, D). Thus, these results suggest that Akt is constitutively activated by mutant KRas-Gly12Asp and is not inhibited by mTOR, whereas in cells that express wild-type KRas or mutant KRas-Gly12Cys, Akt activation is weak, inhibited by mTOR, and is presumably a consequence of stimulation by growth factors but not KRas.

Molecular Modeling Studies of KRas Proteins

Finally, we performed molecular modeling studies of the KRas proteins by using the available crystal structures of HRas (which has approximately 95% sequence identity to KRas) to create homology models of mutant KRas-Gly12Cys and mutant KRas-Gly12Asp, followed by molecular dynamics simulations for structural refinement. KRas interacts with its different downstream effectors by undergoing large conformational changes in the switch I and switch II regions of the protein that surround the amino acids corresponding to codons 12 and 13 (15,16). When

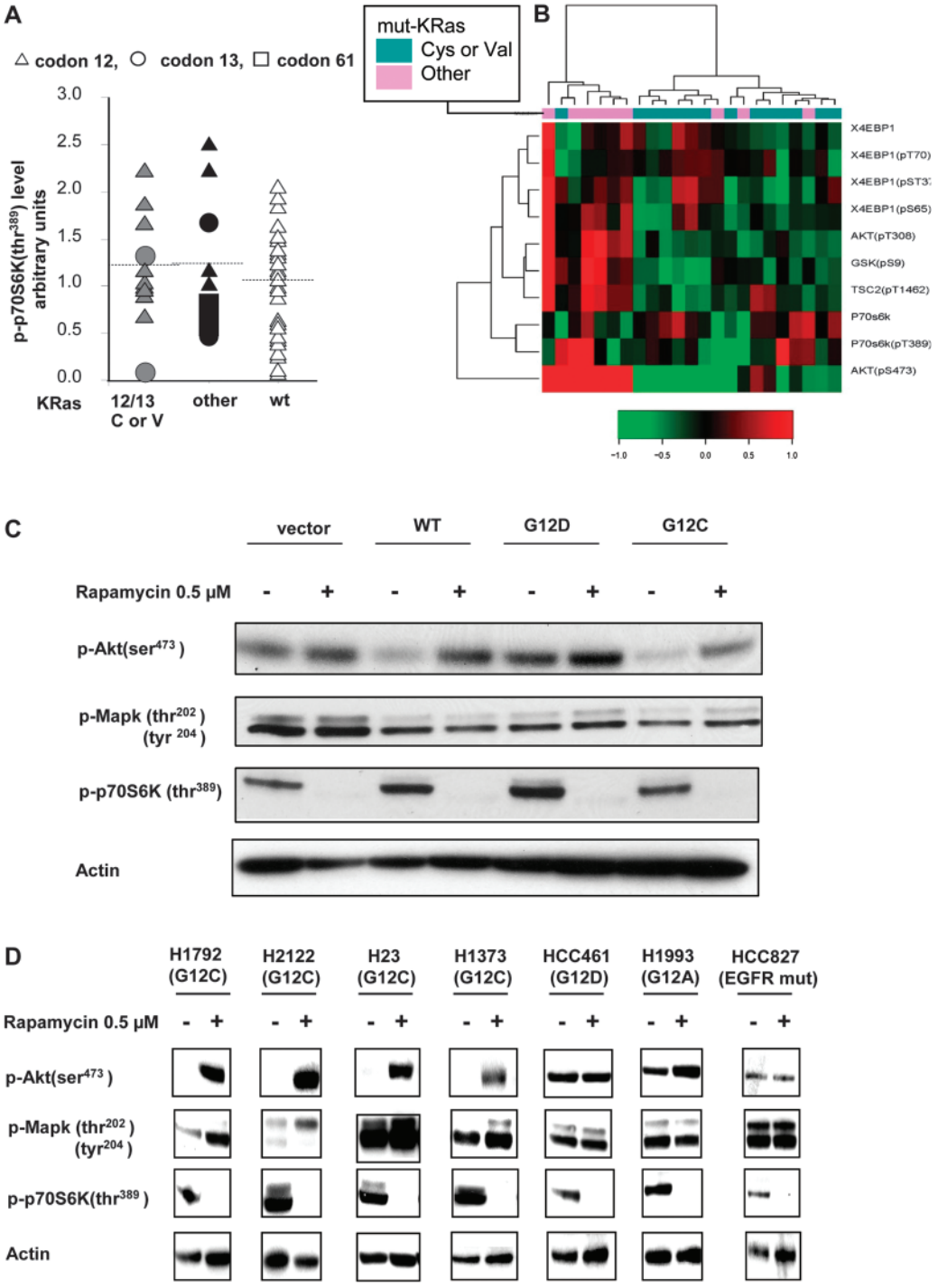

Figure 4. Signaling pathway activation in NSCLC cell lines expressing mutant or wild-type KRas. A) Phospho-p70 S6K (thr^{389}) levels measured by reverse-phase protein array in the panel of 67 NSCLC cell lines grown in medium containing 10% serum. KRas 12/13 C or V = cell lines with mutant KRas-Gly12Cys or mutant KRas-Gly13Cys (n = 13) or mutant KRas-Gly12Val (n = 1); other = cell lines with other mutant KRas (n = 9), wt = cell lines with wild type KRas (n = 45). **Horizontal dotted lines** indicate the mean value for the group. **B**) Two-way hierarchical clustering of NSCLC cell lines based on their expression of phosphorylated Akt and phosphorylated signaling proteins in related signaling pathways. Mutation type is indicated by the **color bar** above the heatmap: 14 cell lines with mutant KRas-Gly12Cys, mutant KRas-Gly13Cys, or mutant KRas-Gly12Val **(green–blue)** and 14 cell lines with other mutant KRas proteins (**pink**). **C**) Immunoblot analysis of Mapk, Akt, and p70 S6 kinase activation in transfected HBECsiP53 cells treated with the mTOR inhibitor rapamycin (0.5 μM) for 16 hours HBECsiP53 cells stably transfected with empty vector (vector), or vector coding for wild-type KRas (WT), mutant KRas-Gly12Cys (G12C), or mutant KRas-Gly12Asp (G12D). **D**) Immunoblot analysis of rapamycin-treated NSCLC cell lines expressing mutant KRas or mutant epidermal growth factor receptor (EGFR). The type of mutation is shown in parentheses.

KRas is bound to PI-3-K, the switch II regions of mutant KRas-Gly12Cys and wild-type KRas exist in a similar conformation that exposes the bound GTP to hydrolysis, thus inhibiting KRas activity. By contrast, a bulky side chain in mutant KRas-Gly12Asp results in electrostatic repulsion on Gly60 in switch II, which allows a hydrogen bond to form between the γ-phosphate of GTP

and Gly61, which protects the nucleotide from hydrolysis, thus stabilizing mutant KRas-Gly12Asp in its active form and activating its bound effector PI-3-K (Figure 5, A). Although PI-3-K and RaLGDS compete for activation by KRas (9), KRas activates these two proteins in very different ways: by direct binding of one KRas molecule to PI-3-K, whereas two KRas molecules form a homodimer to facilitate RaLGDS binding. In the latter case, the interaction of Tyr32 in one KRas molecule with GTP in the other KRas molecule is critical for RaLGDS binding and RalA and RalB activation (16). Our modeling suggests that in mutant KRas-Gly12Asp, the bulky Asp side chain causes steric interference of Tyr32 in switch I, which prevents homodimer formation and RaLGDS binding (Figure 5, B). By contrast, the smaller Cys residue of mutant KRas-Gly12Cys allows homodimer formation and Ral activation. Molecular dynamic and protein–protein docking data (Figure 5, C and D) show the results of these changes, with mutant KRas-Gly12Cys having a higher affinity for binding to RaLGDS and mutant KRas-Gly12Asp a higher affinity for PI-3-K than for RaLGDS.

Discussion

The recently completed BATTLE trial for patients with refractory NSCLC receiving either erlotinib, vandetanib, bexarotene and erlotinib, or sorafenib found that mutant *KRAS* was not associated with overall survival in any of the treatment groups (10). We reanalyzed the BATTLE data to examine associations between mutant KRas with specific amino acid substitutions and patient survival and found that either mutant KRas-Gly12Cys or mutant KRas-Gly12Val was associated with decreased progression-free survival compared with other mutant KRas or wild-type KRas. This is the first study to our knowledge to show an association between mutant KRas amino acid substitutions and response to molecularly targeted therapy in NSCLC.

There is already evidence that mutant KRas amino acid substitution could determine patient response. A study in colon cancer patients receiving EGFR inhibitors revealed that tumors with mutant KRas-Gly12Cys or KRas-Gly12Val are associated with rapid tumor progression and decreased patient survival compared with tumors with other mutant KRas proteins (mostly Gly12Asp) or wild-type KRas (6). A recent study has confirmed that different amino acid–substituted mutant KRas may also affect drug sensitivity of NSCLC patients (22).

Dysregulation of the cell cycle is a well-characterized feature of KRas-mediated tumorigenesis (23,24). Our analysis of tumor transcriptome microarray data from patients in the BATTLE trial provides the first indication to our knowledge that cell cycle signaling differs between the different forms of mutant KRas.

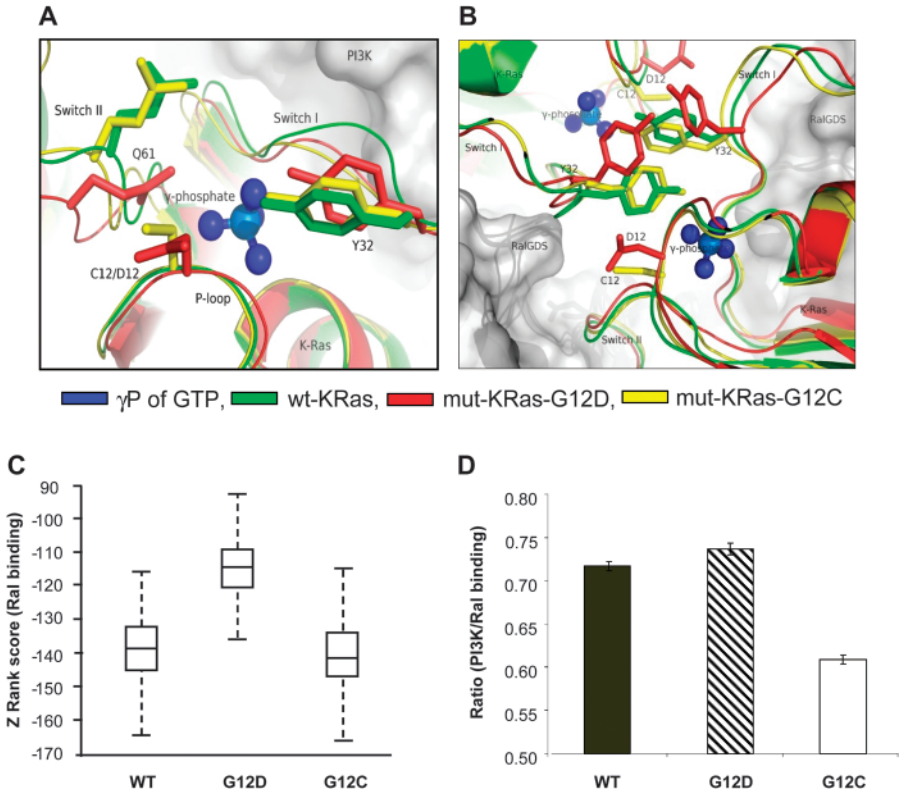

Figure 5. Molecular modeling of the KRas proteins. **A**) KRas with critical amino acid residues (depicted in **stick representations**) in association with phosphatidylinositol 3-kinase (PI-3-K) (depicted as a **gray surface**). In mutant KRas-Gly12Asp (**red**), the Switch II loop is pushed away from GTP (**blue**) by the large side chain of the Asp residue, thereby preventing GTP hydrolysis. Wild-type KRas (**green**) and mutant KRas-Gly12Cys (**yellow**) have similar conformations of Gln61 (Q61) that are open to GTP hydrolysis. Thus, in the presence of PI-3-K, mutant KRas-Gly12Asp is more firmly locked in the GTP-bound state compared with either wild-type or mutant KRas-Gly12Cys and thus constitutively active. **B**) KRas in association with RaLGDS (depicted as **gray surfaces**), the activator of RalA and RalB proteins. KRas exists as a homodimer, with Tyr32 (Y32) of one KRas molecule interacting with the γ-phosphate (**blue**) of another KRas molecule. The bulky side chain Asp residue in mutant KRas-Gly12Asp results in steric clashes with Y32, which impairs dimerization and, thus, binding and activation of RaLGDS. **C**) **Box plots** of predicted binding of wild-type KRas (WT), mutant KRas-Gly12Asp (G12D), and mutant KRas-Gly12Cys (G12C) to RaLGDS. The binding scores were calculated using the ZRANK program for 60 snapshot structures from the molecular dynamics simulations. The ZRANK score estimates the relative binding energy of protein–protein interactions, with a lower score indicating tighter binding. For each box, the **bottom and top lines** represent the 25th and 75th percentiles, respectively, and the **horizontal line** represents the median (50th percentile) of the ZRANK scores. The **error bars** represent the range from the minimum to the maximum of all ZRANK scores collected based on the 60 snapshot structures from the molecular dynamics simulations. **D**) Comparison of predicted binding of the various forms of KRas to RaLGDS with predicted binding of KRas to PI-3-K. The height (*y*-axis) of each panel represents the ratio of averaged binding of KRas to PI-3-K over binding to RaLGDS in terms of ZRANK scores. **Error bars** represent the standard error of the ratios (the corresponding 95% confidence intervals are 0.706 to 0.728 for the WT prediction, 0.723 to 0.751 for the G12D prediction, and 0.599 to 0.619 for the G12C prediction).

Specifically, we found that expression of the cell cycle regulators PLK1, cyclin B, and cyclin E was decreased in tumors with mutant KRas-Gly12Cys or KRas-Gly12Val compared with tumors with other mutant KRas proteins. Our RRPA analysis of a panel of genetically characterized NSCLC cell lines revealed that compared with cell lines expressing wild-type KRas, those with mutant KRas-Gly12Cys or Gly12Val had decreased levels of phosphorylated Akt, whereas those with other mutant KRas proteins had elevated levels of phosphorylated Akt. Transfection of immortalized, p53-deficient human bronchial epithelial HBECsiP53 cells with different mutant KRas expression plasmids also showed that overexpression of mutant KRas-Gly12Cys decreased phospho-Akt levels and increased Ral activation, whereas overexpression of mutant KRas-Gly12Asp increased phospho-Akt levels and decreased Ral activation compared with cells overexpressing wild-type KRas. Moreover, we found that HBECsiP53 cells overexpressing mutant KRas-Gly12Cys had lower Akt signaling, elevated Ral signaling, and increased anchorage-independent growth compared with HBECsiP53 cells overexpressing wild-type KRas. These findings are in agreement with a previous study (25) showing that Ral activation preferentially induces anchorage-independent growth in human cells, whereas Akt or Mek activation has only modest effects. These findings are also consistent with previous observations that when mutant KRas proteins were expressed in the lungs of mice, mutant KRas-Gly12Asp induced Raf and Akt activation (26), whereas mutant KRas-Gly12Cys resulted in Raf and Ral activation but minimal Akt activation regardless of the expression level of the mutant KRas protein (27,28).

Our data showed that mTOR may mediate some of the effects of different amino acid–substituted mutant KRas. We found that many NSCLC cell lines that had minimal Akt activation showed robust activation of the mTOR effector proteins p70 S6 kinase and 4E-BP. We found that inhibition of mTOR with rapamycin in NSCLC cells with mutant KRas-Gly12Cys resulted in decreased expression of p70 S6 kinase and an increase in phospho-Akt levels. The translational regulator mTOR is activated by Akt signaling, in addition to being activated by the Mapk and Ral signaling pathways (21). In addition, p70 S6 kinase downstream of mTOR has been shown to exert a regulatory feedback response that restricts growth factor signaling to the Akt pathway (29). Our results suggest that PI-3-K/Akt signaling is constitutively activated by mutant KRas-Gly12Asp and not subject to mTOR inhibition, whereas in cells expressing wild-type KRas or mutant KRas-GlyG12Cys, Akt activation is growth factor dependent and inhibited by mTOR.

KRas is known to interact with different downstream effectors by undergoing large conformational changes in the switch I and switch II regions of the protein surrounding codon 12 and 13 amino acids (15,16). Our molecular modeling studies showed that mutant KRas-Gly12Cys likely weakens the interaction with PI-3-K, whereas the bulky Asp of mutant KRas-Gly12Asp causes steric interference of KRas homodimer formation and RaLGDS binding, which is not seen with mutant KRas-Gly12Cys. These modeling results are in agreement with the results of our cellular studies showing that mutant KRas-Gly12Asp activated PI-3-K and Mek signaling, but not Ral, whereas mutant KRas-Gl12Cys fails to activate PI-3-K signaling.

The findings of this study showing different mechanisms for signaling through wild-type KRas, mutant KRas-Gly12Asp, and mutant KRas-Gly12Cys are summarized in Figure 6. Wild-type KRas activation results in signaling through Mek. Wild-type KRas has also been shown to activate Akt and RalA/B, although the conditions that dictate which pathway will be activated remain uncertain at this time. The Akt, Mek, and RalA/B pathways have all been shown capable of activating mTOR and its effector p70 S6 kinase, which serves as a negative regulator of growth factor receptor–regulated signaling to Akt. Other KRas effectors are likely also capable of regulating p70 S6 kinase. The KRas-Gly12Asp mutation preferably activates Akt signaling, making growth factor receptor Akt activation unnecessary and p70 S6 kinase inhibition irrelevant. In contrast, the KRas-Gly12Cys mutation preferentially activates RalA/B signaling over Akt and is able to suppress Akt activation through an Akt-independent activation of p70 S6 kinase. Other KRas effectors may also play a role in the signaling, but we have not considered them here.

Our observation that the substitution of different amino acids induces heterogeneous behavior in the KRas protein resulting in different signaling outputs has profound implications for identifying and treating KRAS-driven tumors. For example, it may be necessary to use different combinations of downstream signaling inhibitors when treating tumors with different mutant KRas amino acid substitutions.

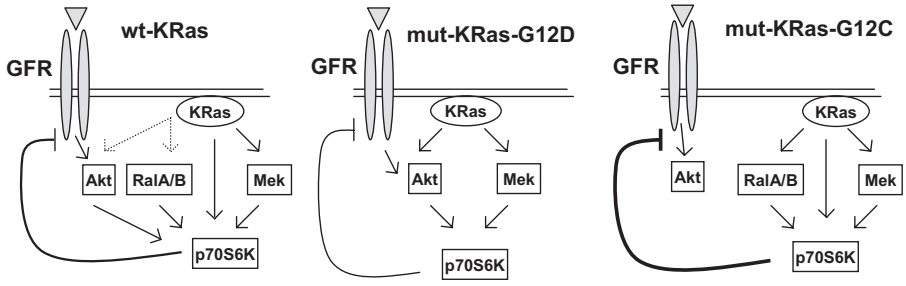

Figure 6. Proposed pathways of signaling by wild-type KRas, mutant KRas-Gly12Asp, and mutant KRas-Gly12Cys showing membrane growth factor receptor (GFR) or wild-type KRas (wt-KRas), mutant KRas-Gly12Asp (mut-KRas-G12D), and mutant KRas-Gly12Cys (mut-KRas-G12C) activation of Akt signaling (acting through PI-3-K), RalA and RalB signaling (acting through RaLGDS), and Mek signaling (acting through c-Raf). Forward transmission of signals is represented by **arrows**. **Solid lines** show established pathways, and **dashed lines** represent possible pathways. P70 S6 kinase (p70S6K) is activated and exerts feedback inhibition on GFR activation of Akt. The thickness of the lines indicates the strength of the feedback inhibition: weak inhibition by mutant KRas-Gly12Asp, moderate inhibition by wild-type KRas, and strong inhibition by mutant KRas-Gly12Cys.

This study focused on the major forms of mutant KRas in NSCLC, namely Gly12Cys (and Gly12Val) and Gly12Asp, and on the downstream signaling pathways involving PI-3-K/Akt, Mek, and Ral. We do not know how other forms of mutant KRas activate the pathways nor do we know how other known KRas downstream pathways [eg, Tiam1/Rac, PLCε/PKC, and Rassf1 (9)] may be affected by mutant KRas. Consequently, our findings that mutant KRas-Gly12Cys and mutant KRas-Gly12Val are associated with overall decreased patient progression-free survival compared with other forms of mutant KRas or wild-type KRas may only be applicable to the types of molecularly targeted agents used in the BATTLE study, which focused broadly on EGFR, VEGF, PI-3-K, and Mek signaling. Future studies will need to explore the role of mutant KRas and signaling pathways in the context of other agents in individual clinical trials.

References

1. Kranenburg O. The KRas oncogene: past, present and future. *Biochim Biophys Acta.* 2005;1756(2):81–82.
2. Raponi M, Winkler H, Dracopoli N. KRAS mutations predict response to EGFR inhibitors. *Curr Opin Pharmacol.* 2008;8(4):413–418.
3. Loriot Y, Mordant P, Deutsch E, Olaussen KA, Soria JC. Are RAS mutations predictive markers of resistance to standard chemotherapy? *Nat Rev Clin Oncol.* 2009;6(9):528–534.
4. Capella G, Cronauer-Mitra S, Peinado MA, Perucho M. Frequency and spectrum of mutations at codons 12 and 13 of the C-K-ras gene in human tumors. *Environ Health Perspect.* 1991;93:125–131.
5. Poorta M, Crous-Bou M, Wark PA, et al. Cigarette smoking and K-ras mutations in pancreas, lung and colorectal adenocarcinomas: etiopathogenic similarities, differences and paradoxes. *Mutat Res.* 2009;682(2–3):83–93.
6. Andreyev HJ, Norman AR, Cunningham D, et al. Kirsten ras mutations in patients with colorectal cancer: a multicenter "RASCAL" study. *J Nat Cancer Inst.* 1998;90(9):675–684.
7. Siegfried JM, Gillespie AT, Mera R, Casey TJ, Keohavong P, Testa JR. Prognostic value of specific KRAS mutations in lung adenocarcinoma. *Cancer Epidemiol Biomarkers Prev.* 1997;6(10):841–847.
8. Hunt JD, Strimas A, Martin JE, et al. Differences in KRAS mutation spectrum in lung cancer cases between African Americans and Caucasians after occupational or environmental exposure to known carcinogens. *Cancer Epidemiol Biomarkers Prev.* 2002;11(11):1405–1412.
9. Cully M, Downward J. SnapShot: Ras signaling. *Cell.* 2008;133(7):1292–1292.e1.
10. Kim ES, Herbst RS, Wistuba II, et al. The BATTLE trial: personalizing therapy for lung cancer. *Cancer Discov.* 2011;1(1):44–53.
11. Shames DS, Girard L, Gao B, et al. A genome-wide screen for promoter methylation in lung cancer identifies novel methylation markers for multiple malignancies. *PLoS Med.* 2006;3(12):e486.
12. Sullivan JP, Spinola M, Dodge M, et al. Aldehyde dehydrogenase activity selects for lung adenocarcinoma stem cells dependent on notch signaling. *Cancer Res.* 2010;70(23):9937–9948.
13. Sato M, Vaughan MB, Girard L, et al. Multiple oncogenic changes (K-RAS[V12], p53 knockdown, mutant EGFRs, p16 bypass, telomerase) are not sufficient to confer a full malignant phenotype on human bronchial epithelial cells. *Cancer Res.* 2006;66(4):2116–2128.
14. Vikis H, Sato M, James M, et al. EGFR-T790M is a rare lung cancer susceptibility allele with enhanced kinase activity. *Cancer Res.* 2007;67(10):4665–4670.
15. Pacold ME, Suire S, Perisic O, et al. Crystal structure and functional analysis of Ras binding to its effector phosphoinositide 3-kinase gamma. *Cell.* 2000;103(6):931–943.
16. Huang L, Hofer F, Martin GS, Kim SH. Structural basis for the interaction of Ras with RalGDS. *Nat Struct Biol.* 1998;5(6):422–426.
17. Phillips JC, Braun R, Wang W, et al. Scalable molecular dynamics with NAMD. *J Comput Chem.* 2005;26(16):1781–1802.
18. Gorfe AA, Grant BJ, McCammon JA. Mapping the nucleotide and isoform-dependent structural and dynamical features of Ras proteins. *Structure.* 2008;16(6):885–896.
19. Seeber M, Cecchini M, Rao F, Settanni G, Caflisch A, Wordom A. A program for efficient analysis of molecular dynamics simulations. *Bioinformatics.* 2007;23(19):2625–2627.
20. Pierce B, Weng ZP. ZRANK: reranking protein docking predictions with an optimized energy function. *Proteins.* 2007;67(4):1078–1086.
21. Dunlop EA, Tee AR. Mammalian target of rapamycin 1: signaling inputs, substrates and feedback mechanisms. *Cell Signal.* 2009;21(6):827–835.
22. Garassino MC, Marabese M, Rusconi P, et al. Different types of K-Ras mutations could affect drug sensitivity and tumour behaviour in non-small-cell lung cancer. *Ann Oncol.* 2011;22(1):235–237.
23. Fan J, Bertino J. KRas modulates the cell cycle via both positive and negative regulatory pathways. *Oncogene.* 1997;14(21):2595–2607.
24. Drosten M, Dhawahir A, Sum E, et al. Genetic analysis of Ras signaling pathways in cell proliferation, migration, and survival. *EMBO J.* 2010;29(6):1091–1104.
25. Hamad NM, Elconin JH, Kamoub AE, et al. Distinct requirements for Ras oncogenesis in human versus mouse cells. *Genes Dev.* 2002;16(16):2045–2057.
26. Tuveson DA, Shaw AT, Willis NA, et al. Endogenous oncogenic KRas (G12D) stimulates proliferation and widespread neoplastic and developmental defects. *Cancer Cell.* 2004;5(4):375–387.
27. Floyd HS, Farnsworth CL, Kock ND, et al. Conditional expression of the mutant Ki-Ras G12C allele results in formation of benign lung adenomas: development of a novel mouse lung tumor model. *Carcinogenesis.* 2005;26(12):2196–2206.
28. Dance-Barnes ST, Kock ND, Floyd HS, et al. Effects of mutant human Ki-Ras (G12C) gene dosage on murine lung tumorgenesis and signaling to downstream effectors. *Toxicol Appl Pharmacol.* 2008;231(12):77–84.
29. O'Reilly KE, Rojo F, She QB, et al. mTOR inhibition induces upstream receptor tyrosine kinase signaling and activates Akt. *Cancer Res.* 2006;66(3):1500–1508.

Funding

National Institutes of Health Grants (CA155196 to R.H., CA160398 to G.P.); DOD grant (W81XWH-6-1-0303 to W.K.H.); MD Anderson's Cancer Center Support Grant (P30 CA016672); and gift from the Perot Foundation (G.P.).

Notes

The study sponsors had no role in the design of the study; the collection, analysis, or interpretation of the data; the writing of the article; or the decision to submit the article for publication.

Affiliations of authors: Department of Experimental Therapeutics (NTI, LC, SZ, MFA, GP), Department of Thoracic Head and Neck Medical Oncology (LAB, ESK, PS, GRB, AT, XT, VP, SML, WKH, RSH, IIW, JVH), Department of Biostatistics (JJL, SL, JW, LD, KRC), and Department of Pathology (IIW); The Hamon Center for Therapeutic Oncology Research and Simmons Cancer Center, University of Texas Southwestern Medical Center, Dallas, TX (JEL, JDM).